Journal of Manufacturing Processes 41 (2019) 56–65

Contents lists available at ScienceDirect

Journal of Manufacturing Processes

journal homepage: www.elsevier.com/locate/manpro

Comparative study on the joining performance of TiH_2 and ZrH_2 modified $AgCu_{28}$ brazing alloys with pulsed laser welding-brazing

Yonggui Huang[a], Guoxing Liang[a,*], Ming Lv[a], Mohammed Al-Nehari[a], Donggang Liu[a], Guang Li[a], Chun Xiao[b]

[a] College of Mechanical and Vehicle Engineering of Taiyuan University of Technology, Shanxi Key Laboratory of Precision Machining, Taiyuan, 030024, Shanxi, People's Republic of China

[b] Customer Service Center of SEPC of SGCC, Taiyuan, 030008, Shanxi, People's Republic of China

ARTICLE INFO

Keywords:
Laser welding-brazing
AgCu-based alloy powder
Active elemental Zr
Mechanical alloying
Microstructure
Tribology performance

ABSTRACT

Brazed alloys between cubic boron nitride (cBN) grits and matrix extremely affect the service life of the grinding wheel. The aim of this study was to investigate the addition of elemental Zr to improve the connection effect of alloys. The plates of pure titanium (Ti) Gr. 1 and AISI 1045 steel had been applied to conduct the welding-brazing experiments with active brazing alloys of $AgCu_{28}$-4.5Ti and $AgCu_{28}$-4.5Ti-4Zr. Brazing alloys was heated with an Nd:YAG pulsed laser welding-brazing system under inert argon gas atmosphere. Transition zones between the brazed alloys and matrices were investigated with scanning electron microscope (SEM), energy dispersion spectrometer (EDS), and X-ray diffraction (XRD) analyses. In addition, hardness of the brazed layer was analyzed as well as tribology. The results showed that the active element, zirconium (Zr), significantly accelerated the bidirectional diffusion and improved the gradient evolution of the main elements in the transition zones. Compared to Zr-free brazing alloys, the active element, Zr, inhibited the overproduction of the hard-brittle phase of Cu_3Ti and formed other intermetallic compounds, such as $AgZr_2$ and $Cu_{10}Zr_7$, which were beneficial to the metallurgical joint. A brazed layer with a lower friction coefficient, a more uniform hardness distribution, and better ductility was obtained, though the wear resistance slightly decreased. A solid solution product of Zr-Cu was formed during laser welding-brazing process, which strengthens the brazed layer and improves its overall performance.

1. Introduction

Due to excellent physicochemical properties, such as having high hardness, thermal stability, superior thermal conductivity, corrosion resistance, and the wear resistance [1–3], cubic boron nitride (cBN) grinding wheels are becoming one of the most potential tools in modern engineering applications. However, some practical problems have become increasingly obvious with the wide application of super-abrasive cBN tools.

The metallurgical incompatibility and physical mismatch between abrasive particles and metal matrices [4] are the main problems of this technology. One way to circumvent these is to first coat a thin metal layer on the surface of the cBN abrasive particles and then connects them with the substrate under the action of brazing alloys. Therefore, a study of the coated cBN and its metal matrix is essentially transformed into an investigation of the connection of dissimilar materials. In fact, the joining of dissimilar materials is a challenging task that modern manufacturers have to face [5,6]. Some unsolved issues remain, in particular, the degradation of mechanical properties that mainly result from the thermal stress in the joint field and the formation of brittle intermetallic phases in the joining process. For example, the thermal joining of aluminum (Al) and titanium (Ti) has a metallurgical challenge due to the unavoidable formation of brittle intermetallic compounds [7,8]. Meco et al. [9] found that the number of intermetallic phases determined the joint strength in the joining of structural steel to Al alloy. In order to minimize the formation of brittle intermetallic phases, some studies had proposed and demonstrated a variety of approaches. Elrefaey et al. [10] indicated that the intermediate materials play a dominating role in joining steel alloys to Ti, as they inhibit the brittle intermetallic compounds and thus accommodate the chemical compatibilities between Ti and steel alloys. Lee et al. [11] obtained a strong bonding joint of Ti Gr. 2 (ASTM grade 2) to stainless steel STS

* Corresponding author.
E-mail addresses: huangyonggui0003@link.tyut.edu.cn (Y. Huang), liangguoxing@tyut.edu.cn (G. Liang), lvming@tyut.edu.cn (M. Lv), mba2050@yahoo.com (M. Al-Nehari), liudonggang0012@link.tyut.edu.cn (D. Liu), liguang0010@link.tyut.edu.cn (G. Li), tyutxiaochun@163.com (C. Xiao).

https://doi.org/10.1016/j.jmapro.2019.03.026
Received 27 October 2018; Received in revised form 3 February 2019; Accepted 22 March 2019
Available online 29 March 2019
1526-6125/

using an engineered interlayer structure. The results showed that suitable supplementary composite brazing alloys containing at least two layers of different elements were needed. Silver (Ag) and its alloys are widely applied as interlayers in the diffusion bonding of Ti and different type of steels. Atasoy et al. [12] investigated the joining of pure Ti to low-carbon steel using an Ag interlayer and they found that Ag cannot form a brittle intermetallic layer with the main elements in steel. Shen et al. [13] determined that although a Ti-Ag phase was formed at the connection interface, it was not as brittle as many other Ti-based intermetallics and it had considerable ductility. Zhang et al. [14] determined that using copper (Cu) as an interlayer can greatly reduce amounts of the Ti-Fe intermetallic material and subsequently realize the effective combination between Ti alloys and stainless steel. Ding et al. [15] studied a kind of active brazing alloy, Ag-Cu-Ti, and obtained bonding joints due to good wettability of the alloy and using an appropriated brazing temperature. Xiao et al. [16] studied the effects of zirconium (Zr) addition on the microstructure and properties of Cu-Ag-Ti alloys. The results indicate that adding Zr to this alloy can decrease the amount and size of the acicular phase Cu_3Ti, and the oxidation resistance of the $Cu_{50}Ag_{46\text{-}x}Zr_xTi_4$ alloys was much better than the alloys without Zr. Furthermore, Zr had a more negative Gibbs free energy than Ti.

Likewise, thermal-stress mismatch is another factor that restricts joining. Some researchers have focused on joining dissimilar materials by different methods, such as solid-state [17,18], reactive wetting [19,20] and friction stir welding joining processes [21]. However, these methods are not suitable for joining tailored blanks such as cBN tools due to the limitations of special joint configuration or whole heating. Dezellus et al. [22] demonstrated that lowering the brazing temperature was the key to limiting the effect of mismatch between the coefficients of thermal expansion of joining metals. As a heat source in materials processing, laser welding-brazing technologies have good characteristics for dissimilar joining, such as high energy density, rapid heating-cooling velocity, and accessibility to the heating zone [23,24], lowering the brazing temperature, restraining the damage to the matrices because of a smaller heating area [25]. In addition, the laser welding-brazing method to attach metallurgical non-fitting partners to each other can also effetely suppress the growth of brittle intermetallic compounds [26], which leads to desirable mechanical properties [27,28].

The wear of brazed alloys between abrasive particles and the matrix is another important factor affecting the service life of cBN tools in application [29]. A brazed grinding wheel has a larger inter-grit chip-accommodation volume [30,31] because the average crystal exposure from the bond level is 70–80% of the grit height [32]. Thus, large amounts of grinding debris are filling in the gap of the grinding grains due to the limitation of grinding area. Friction and extrusion happen repeatedly among the grinding debris and brazed alloys. Plastic deformation then occurs and is associated with the formation of surface and subsurface micro- and macro-cracks due to the high grinding temperature [33]. These will aggravate the wear of the brazed layer and lead to the final drop of the abrasive grains. While, Most of the previous studies on tribological properties focused on the friction and wear behavior of cBN abrasives grits after brazing. Ding et al. [15] studied the wear behavior of Ag-Cu/Ti active brazing alloys joining cBN abrasives with medium-carbon steel, and the results evidently suggested that the joining between cBN abrasive grains and Ag-Cu/Ti powder is stronger than the own strength of the molten filler alloy. Bhaduri et al. [34] studied the tribological behavior of TiN and MoS_2-Ti composite coating for enhancing the performance of monolayer cBN grinding wheels. The results showed that MoS_2-Ti composite coating, with a hard TiN underlayer deposited on brazed layers, exhibited better tribological performance in terms of lower coefficients of friction and depth of worn track. The coating could effectively prevent the breakage and pulling out of cBN abrasive grains, greatly improve the tool performance. In addition, Xu et al. [35] and Wang et al. [36] studied the residual stresses and wear evolution of single-brazed cBN abrasive grit by using finite element analysis. Zhou et al. [37] further considered the consecutive action for two abrasive grains. However, the properties of brazed alloys were not taken into account, and detailed investigations on the tribological properties for brazed alloys were scarce in publications.

In order to reduce the difference of thermal performance among new hard-brittle phases and substrates, as well Ti-coated cBN particles, and, ultimately, obtain a metallurgical joint with high wear resistance, Ti Gr. 1 was used instead of the coated cBN. Using $AgCu_{28}$-4.5Ti and $AgCu_{28}$-4.5Ti-4Zr brazing alloys, the connection between AISI 1045 steel and Ti was investigated in this work. Elemental diffusion behavior at the fusion zone together with interfacial intermetallic compounds was studied. The friction and wear behavior of these brazed layers sliding against GCr15 steel under dry sliding conditions was investigated as well.

2. Materials and methods

2.1. Materials

Commercially available eutectic $AgCu_{28}$, TiH_2, and ZrH_2 (Tianjiu Metal Materials Co., LTD, Changsha, China, 200–300 mesh, 99.8% purity) were blended to produce the raw elemental powders. The powders were mechanically alloyed with a QM-QX 04 all-round planetary ball mill (Nanjing Nanda Instrument Plant. Nanjing, China) in stainless steel grinding media and the weight ratio of ball-to-powder was 10:1. The milling time was 24 h, and the alloying process was performed in the protective atmosphere of dry argon with a rotation speed of 400 rpm. The powders were taken out for characteristic analysis. The precursor powders and the as-prepared brazing alloys are shown in Fig. 1. A1 and A2 denote alloyed powder of $AgCu_{28}$-4.5Ti and $AgCu_{28}$-4.5Ti-4Zr, correspondingly, which could be regarded as active brazing alloy. The main components, proportion (wt.%), and some physical parameters of $AgCu_{28}$-xTi-yZr are given in Table 1.

AISI 1045 steel bars were prepared with a length of 10 mm, a width of 10 mm, and a thickness of 2 mm, as well as Ti Gr. 1 bars for laser welding-brazing. The physicochemical properties of two bars are listed in Table 2. The surface of the bar was ground, polished, and then ultrasonically cleaned with acetone.

2.2. Experimental set up and parameters

Brazing alloys were preset on the surface of the matrix specimens along the welding-brazing direction, as shown in Fig. 2, and were blended with anhydrous ethanol to avoid the alloy particle falling. The width of preset alloy layer was slightly less than the diameter of the laser spot. Consequently, a small amount of laser energy was enough to realize the connection between the preset layer and matrix. An Nd:YAG pulsed laser machine was employed in the welding-brazing test, with a lens focal length of 80 mm and a laser spot diameter of 2 mm. Argon (99.99% purity) was used as a shielding gas with a flow rate of 20 L/min. Based on preliminary experiments, a laser pulse current of 200 A, a pulse width of 6 ms, a pulse frequency of 15 Hz, and a scanning speed of 500 mm/min were selected and held constant in this experiment.

After the welding-brazing operation and ultrasonic cleaning of the brazed surfaces were completed, the specimens were cut normal to the welding direction to obtain its subsequent cross-section. Microstructure observations of the specimens at the transition zone were performed with a VEGA 3 SBH scanning electron microscope (SEM). And the compositional analyses of the certain phases were detected by using an Oxford X-ray energy dispersive spectroscopy (EDS) system. An X-ray diffractometer (XRD) with Cu-K radiation (k = 0.154 nm) was used to identify the phases in the transition zones. Vickers hardness was measured on the polished surfaces by using a diamond pyramid indenter under a load of 9.807 N for 15 s by HMV-G micro hardness tester. More

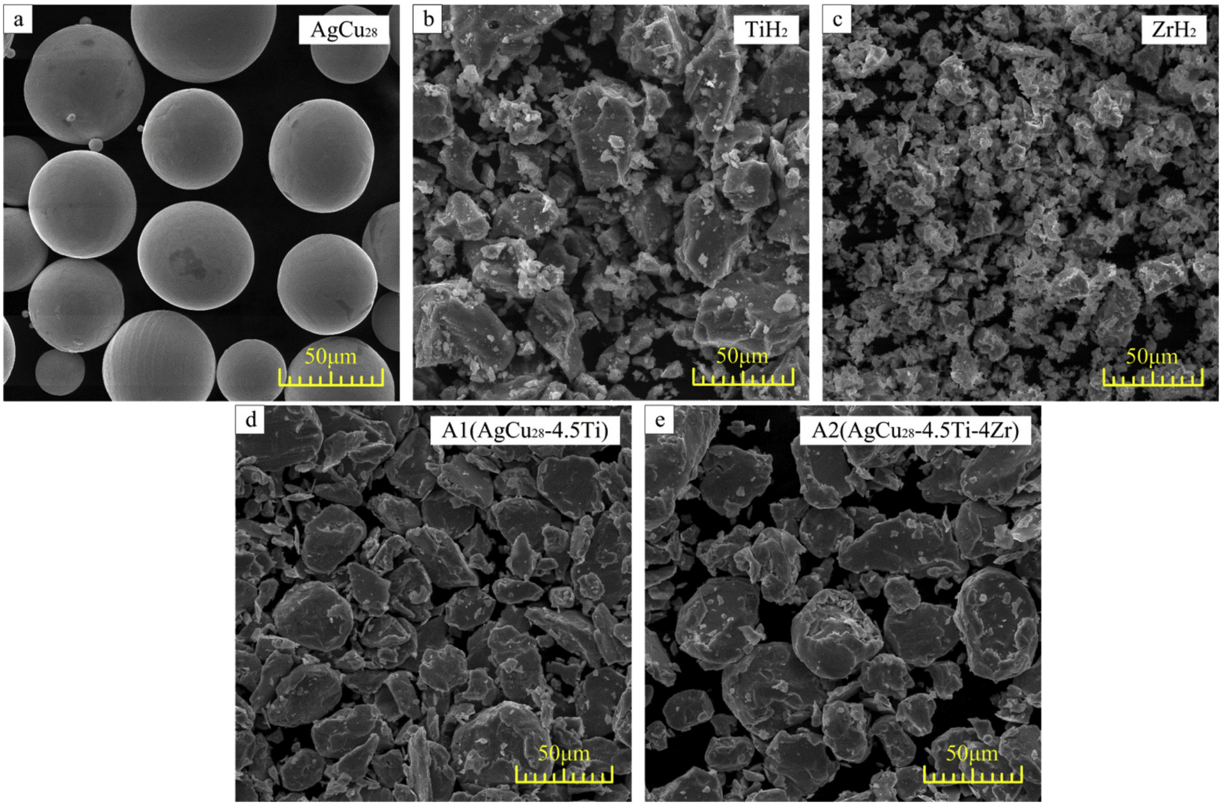

Fig. 1. The SEM micrograph of powders: (a) $AgCu_{28}$; (b) TiH_2; (c) ZrH_2; (d) A1 ($AgCu_{28}$-4.5Ti); (e) A2 ($AgCu_{28}$-4.5Ti-4Zr).

than five positions were randomly selected for tests under the same experimental conditions. The tribological tests were carried out on a CFT-I multi-functional comprehensive performance tester (Zhong Ke Kai Hua Corporation, Lanzhou, China). In the form of reciprocating tribotester with a ball-on-plate configuration, and the material of the grinding ball was GCr15 steel with a diameter of 5 mm, a Rockwell hardness of 63 HRC and the chemical compositions were determined, as shown in Table 3. The mean value of the sliding speed was 12 m/min, and the normal load was 100 N. The testing time was 30 min, and the sliding stroke was 4 mm. All the tests were conducted at least three times to ensure repeatability.

3. Results and discussion

3.1. Macroscopic feature

Obtained macroscopic features on the top view of the specimens B1 (Matrix: AISI 1045 steel; Brazed alloy: $AgCu_{28}$-4.5Ti) and B2 (Matrix: AISI 1045 steel; Brazed alloy: $AgCu_{28}$-4.5Ti-4Zr) are presented in Fig. 3. The effective width of the brazed layer on the specimen B1 is consistent with that of the brazed layer on B2. The brazed layer on B1 seems to be an asperity surface and the scale-like shapes on the seam can be obviously observed. A large number of granular alloys spattered can also be found and attach to the welding-brazing seam. It can be explained that a small amount of incomplete molten powders coerced by the melt produces the granular alloys and results in decreasing spreading of liquid melt in the laser welding-brazing process. Unlike traditional heat source, such as furnace brazing, flame brazing and induction brazing, et al., laser heating has the characteristics of the sudden heating and cooling rate. As the spot irradiates on the powder, heated preset layer begins to transfer the heat from preset layer to the matrix. Most of the powders are molten to generate the liquid phase. Some material with high-melting point, such as Ti, is not enough heated to produce the liquid-solid two-phase and becomes the incomplete molten powder after cooling. A little material with low-melting point is burnt and vaporized. The expansion of the metal from solid to gas breaks the liquid phase together with the incomplete particles and shapes the granular alloys spattering around the seam. The detailed morphology of the particle is given in the magnified picture of Fig. 3 (a). The overall morphology of the brazed A2 is greatly improved. The scale-like-shape layer becomes smooth and its depth of superposition among the stripes appears to be smaller than that of the brazed A1 due to addition of Zr. Additionally, a small amount spatter can hardly be found on the brazed layer. The perfect spreading performance of the alloy is realized in the welding-brazing process, as shown in the magnified picture of Fig. 3 (b). The wettability of brazed A2 to the matrix is improved. And the

Table 1
Active brazing alloys (A1 and A2) with the nominal composition and some important properties [38].

Code	Alloy	Nominal composition (wt %)			Coefficient of thermal expansion
		$AgCu_{28}$	TiH_2	ZrH_2	
A1	$AgCu_{28}$-4.5Ti Ag-Cu(Eutectic) + 4.5%TiH_2 manually added	95.5	4.5	0	18.5×10^{-6} /K
A2	$AgCu_{28}$-4.5Ti-4Zr Ag-Cu(Eutectic) + 4.5%TiH_2 + 4%ZrH_2 manually added	91.5	4.5	4.0	18.2×10^{-6} /K

Table 2
The physicochemical properties of the AISI 1045 steel [39] and Ti Gr. 1.

Materials	Small amount of composition (%)										Melting point (K)	Coefficient of thermal expansion(/K)
AISI 1045 steel	Fe	C	P	Si	Ca	Mn	Mo	Ni	Cr	W	1808	14.67×10^{-6}
	Bal.	0.46	0.03	0.31	0.4	0.65	0.08	0.39	0.04	< 0.01		
Ti Gr. 1	Ti	C	Fe	N	H	O					1941 ± 10	8.36×10^{-6}
	Bal.	≤0.10	≤0.30	≤0.05	≤0.015	≤0.25						

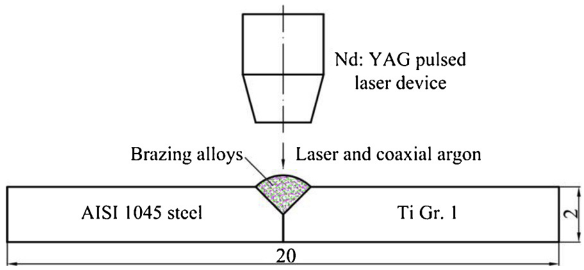

Fig. 2. Schematic diagram of laser welding-brazing.

brazed connection strength would be enhanced. It suggests that the addition of Zr is a main factor affecting the spreading behavior and improves prominently the wettability of the AgCu-based brazing alloys.

3.2. Intermetallic reaction layer

The SEM macrographs and micrographs of the welding-brazing interfaces among brazed layers, AISI 1045 steel matrix, and Ti Gr. 1 matrix are shown in Fig. 4. It can be observed that the welding-brazing connections between two matrices have been achieved. The compact structure of brazed layers have been generated in the connection zone and the average minimum thickness is about 1375 μm and 1136 μm, respectively. As for the brazed seams between two matrices, an obvious distinction can be measured in the height of brazed alloys A1 and A2. It is implied that the compactness of A1 after welding-brazing is lower than that of A2. More uniform structure of the layer and a better wettability with two types of the matrix could be obtained in the specomen of A2 during the laser brazing process.

As shown in Fig. 4(b) and (f), a belt transition zone at the interface is formed between A1 and AISI 1045 steel and its width is about 5 μm. The elements in the transition zone are mainly includes Fe, Ti, Cu and Ag. Comparing two areas of the brazed layer and the transition area, the content of elemental Fe presents a large gradient evolution. The content of Ti in the transition zone is extremely higher than that of in the brazed layer, also a little bit higher than that of in the subsurface zone. The results show that a unidirectional diffusion at the interface junction of A1 and AISI 1045 steel have been occurred from the brazed alloys to the matrix. The main components in the transition zone have been created due to a large amount of active elemental Ti being enriched at the interface. Furthermore, some elemental Ti diffused to the subsurface zone of AISI 1045 steel matrix. These diffusions generated would be beneficial to improving the bonding strength. Combined with the results shown in Fig. 5(a), the main components of the transition layer are intermetallic compounds of $Cu_{0.8}Fe_{0.2}Ti$ and $Cu_{40}Fe_{60}$. Therefore, the metallurgical-chemical reaction between the alloys and the AISI 1045 steel matrix has been occurred in the welding-brazing process. The reliable interfacial connection will be obtained.

In Fig. 4(c) and (g), the transition zone with a width of 45–55 μm can be measured close to the side of the brazed alloys at the interface between A1 and Ti Gr. 1. It is primarily composed of active elemental Ti and the basic elements Cu and Ag. In the transition zone, the enrichment effect of the element can be observed obviously. Elemental Ti rooting in the alloys and the matrix of Ti Gr. 1 forms a continuous gradient evolution region. The content of Cu in the brazed alloys is also enriched to the side of Ti Gr. 1. Its content is less than that of Ti and higher than that of Ag. As a matter of fact, the content of Cu (26.74 wt.%) is lower than that of Ag (68.76 wt.%), higher than that of Ti (4.5 wt.%) in A1. In a sense, elemental Ti plays an active role in the transition zone in the laser welding-brazing process. Depending on the distribution characteristics of Cu and Ag in Fig. 4 (g), Ti has more affinity to Cu than to Ag in the brazed alloys. And it is more inclined to react with Cu elements. The reactants are mainly Cu_3Ti compounds in terms of the XRD test results shown in Fig. 5(a). Because of a large amount of Cu_3Ti compound generated in the transition zone, further reactions between Ti and Ag elements in the brazed alloys are prevented to some extent. Therefore, a small quantity of $AgTi_3$ compound has been produced.

Fig. 4 (d) and (e) shows the microstructure of the brazed layer in the center and near the matrix, respectively. It is mainly consistent with Ag-Cu phases that dispersed with Cu-Ti particles in the middle part. With the enrichment of Ti into the transition zone, the content of Ti in the composition increases near to the matrix, which leads to the increasing of Ag-Ti compound, and some α-Ag are dissolved in the brazed layer according to the EDS test results.

As shown in Fig. 4 (i) and (m), a relatively narrow belt transition zone with a width of 6–10 μm formed at the interface between the brazed A2 and AISI 1045 steel. Compared to A1, the distribution curves of the main elements at the transition zone tend to be flat with the addition of appropriate amounts of Zr, and there is no sharp gradient evolution. The contents distribution of Fe, Ti, Zr, and Ag illustrates that the bidirectional diffusion of elements exists in the interface between the brazed A2 and AISI 1045 matrix. It can be asserted that the combination of AgCu-based active brazing alloys and AISI 1045 steel has been effectively promoted by Zr. According to the XRD analysis results shown in Fig. 5 (b), intermetallic compounds are represented by Fe_4Cu_3 and $ZrFe_2$ formed in the interface transition zone.

It can be seen in Fig. 4 (j) and (n), the transition zone with an approximate width of 60 μm is formed between the brazed A2 and Ti Gr. 1 interface, and distributed close to the side of the brazed alloy as well. The elements at the zone are mainly composed of active elemental Ti and Zr as well as Cu and Ag in accordance with the EDS results. The active elements of Ti and Zr from the brazed alloys are enriched to the transition zone, and Ti both from the brazed alloy and Ti Gr. 1 form a continuous gradient evolution. The distribution of Zr is accumulated in the transition zone, and its content in this area is slightly lower than that of Ti, and higher than that of Cu and Ag. Such a phenomenon is consistent with the elemental content of Zr in brazing alloys as well as its interfacial enrichment. It is worth noting that the distribution curves

Table 3
Chemical compositions of GGr15 Steel. (wt.%).

C	Si	Mn	P	S	Ni	Cr	Mo	Cu
0.95˜1.05	0.15˜0.35	0.20˜0.40	≤0.027	≤0.02	≤0.03	1.3˜1.65	≤0.10	≤0.025

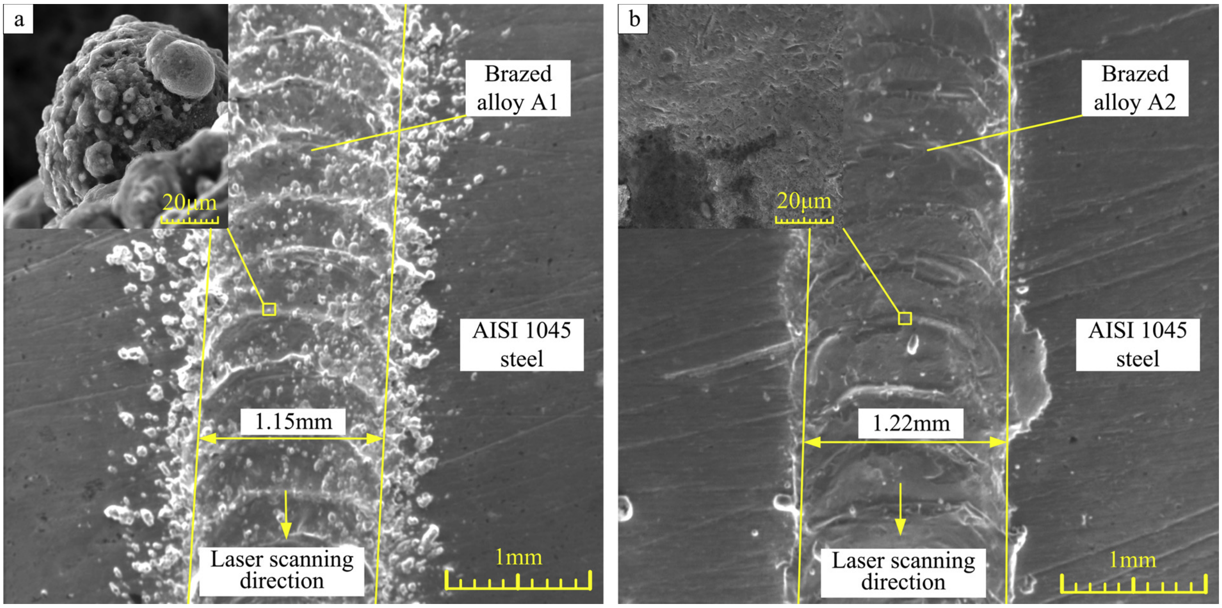

Fig. 3. The macroscopic features of brazed alloys on AISI 1045 steel substrate: (a) B1 (Matrix: AISI 1045 steel; Brazed alloy: $AgCu_{28}$-4.5Ti); (b) B2 (Matrix: AISI 1045 steel; Brazed alloy: $AgCu_{28}$-4.5Ti-4Zr).

of the active elemental Ti and Zr tend to be smooth, and the gradient trend appears to be decreased comparing to the transition zone between the brazed A1 and Ti Gr. 1. This indicates that the metallic compatibility at the interface is improved. And the addition of Zr is beneficial to promote the metallurgical reaction between the AgCu-based brazing alloys and Ti Gr. 1, which will lead to a more reliable welding-brazing connection.

Although still the hard-brittle phase of Cu_3Ti existing in A2, the diffraction intensity is greatly weakened. Diffraction peaks such as $AgZr_2$ and $Cu_{10}Zr_7$ can be found in the XRD test results, as shown in Fig. 5(b). It is claimed that the formation of $Cu_{10}Zr_7$ phases could lead to higher Young's modulus of the composite as well as the ductility [40]. Additionally, the published [41] stated that the uniform layers are apt to be produced due to the fusion of intermetallic compound $AgZr_2$ and the surface of brazed layer becomes smooth. Therefore, the addition of Zr not only inhibited the formation of Cu_3Ti in the reaction layer [16], but also improved the ductility of the brazed layer and smoothed the surface. The solid solution (Zr, Cu) is also detected in the products of A2 and could cause a solution-strengthen effect on the brazed layer, which helps improve the mechanical properties of the material. Although very small amounts Ti-Ag phases were detected, it has been reported that these phases are considerably ductile rather than brittle as the major phases of Ti-based intermetallic compound [42]. In addition, an intermetallic compound of $AgCu_4Zr$ was not detected in the products. It is stated that this type of compound could enhance wear resistance [43]. A complex connection mechanism must be occurred during the laser welding-brazing process, such as phase transition, diffusion and reaction among the various elements, et al.

The microstructures of the brazed layer close to the matrix and in the central part are also shown in Fig. 4(k) and (l), respectively. The compositions are different from that of A1, especially in the central part. The size of the dispersed phase is increased in the structure of the brazed alloy. Combined with the results of EDS and XRD analysis, it can be concluded that part of Cu_3Ti in the layer is replaced by the newly formed Zr-containing phases.

3.3. Micro vickers hardness

The micro Vickers hardness of the two specimens welding-brazing with brazing alloys A1 and A2 in the same condition have been obtained, as shown in Fig. 6. For specimen B1, the mean value and maximum value of Vickers hardness have been monitored in five tests, which they are 505.4 N/mm^2 and 594 N/mm^2, respectively. And for specimen B2, the values are 461 N/mm^2 and 482 N/mm^2. It can be deduced from comparison results that the mean hardness value of specimen B1 is 44.4 N/mm^2 higher than that of specimen B2. The overall hardness of the brazed alloys decreases by 8.8% with the addition of 4.0 wt.% Zr. It can be explained that Zr inhibited the formation of the hard-brittle Cu_3Ti in the reaction layer. Although the newly formed $AgZr_2$ and $Cu_{10}Zr_7$ phases are detected in brazed A2, no remarkable effect on hardness could be found due to the increased ductility properties of two types of phases. Moreover, it is also noted that the discrete degree in the hardness of the specimen B1 is much higher owing to the large amounts of Cu_3Ti intermetallic compound. The larger discrete degree in the hardness of the specimen B1 indicates a poor composition uniformity of the brazed layer. To be sure, the existence of hard-brittle intermetallic compounds of Cu_3Ti is a key factor influencing the composition uniformity of the brazed alloys. In general, to a certain extent, the physicochemical properties of the brazed layer will be improved by adding a reasonable amount of the elemental Zr. Hardness been reduced with the addition of the elemental Zr in the brazed layer, it is still higher than that of the AISI 1045 steel matrix (approximately 360 N/mm^2 [44]).

3.4. Friction and wear performance

3.4.1. The frictional coefficient

Fig. 7 shows the tribological test results of B1 and B2. Each experimental specimen has been conducted for three trials under the same conditions.

Upon comparing results, the figure illustrates that the friction coefficient curves are relatively smooth. The oscillation amplitude decreases with a moderate amount of Zr element adding in the alloy powder before laser welding-brazing, such as B2. The structure and mechanical properties of brazed layers could be partially evaluated with the results of friction coefficient. Certainly, a hard intermetallic compound existed in the brazed layer would induce the non-uniform composition before adding the elemental Zr. Contacting or separating generated repeatedly between the grinding ball and the intermetallics leads to oscillation of the friction coefficient during the sliding tests. A

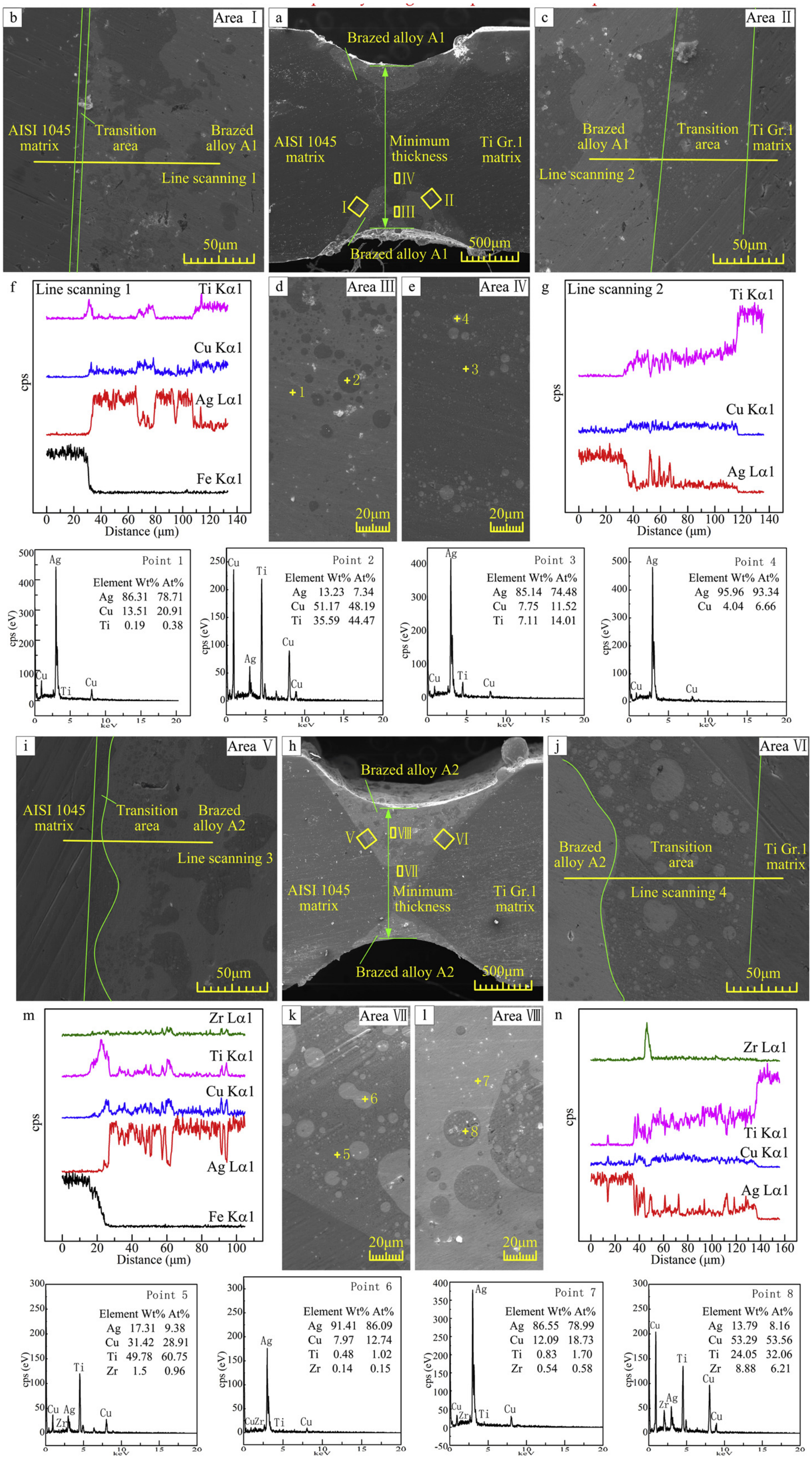

Fig. 4. The SEM macrographs and micrographs of bonding surface: (a) The cross section of brazed A1; (b) The transition zone of AISI 1045 to A1; (c) The transition zone of Ti Gr.1 to A1; (d) The micrograph of brazed A1 in center; (e) The micrograph of brazed A1 near the matrix; (f) The line scanning of AISI 1045 to A1 transition zone; (g) The line scanning of A1 to Ti Gr.1 transition zone; (h) The cross section of brazed A2; (i) The transition zone of AISI 1045 to A2; (j) The transition zone of Ti Gr.1 to A2; (k) The micrograph of brazed A2 in center; (l) The micrograph of brazed A2 near the matrix; (m) The line scanning of AISI 1045 to A2 transition zone; (n) The line scanning of A2 to Ti Gr.1 transition zone.

smoother curve of the friction coefficient indicates a flatter layer fabricated. The friction coefficient (μ) between two smooth bodies under sliding elasticity conditions can be expressed as follows [45,46]:

$$\mu = A\frac{\tau}{P^{1/3}}\left(\frac{3}{4E'}\right)^{2/3} \tag{1}$$

Where A is constant defined by two contact bodies, τ is shear stress

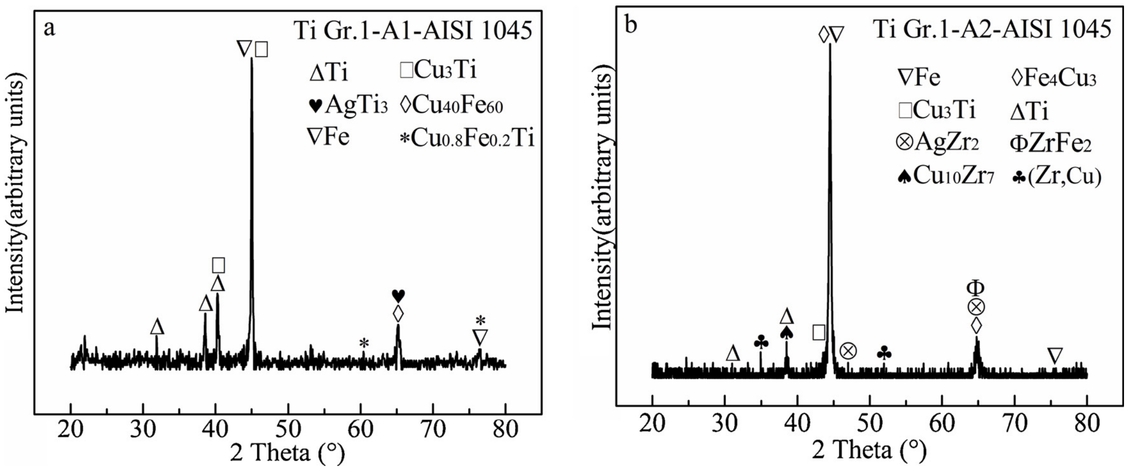

Fig. 5. XRD patterns for Intermetallic reaction layer of brazed alloys: (a) Ti Gr. 1-A1 ($AgCu_{28}$-4.5Ti)-AISI 1045; (b) Ti Gr. 1-A2 ($AgCu_{28}$-4.5Ti-4Zr)-AISI 1045.

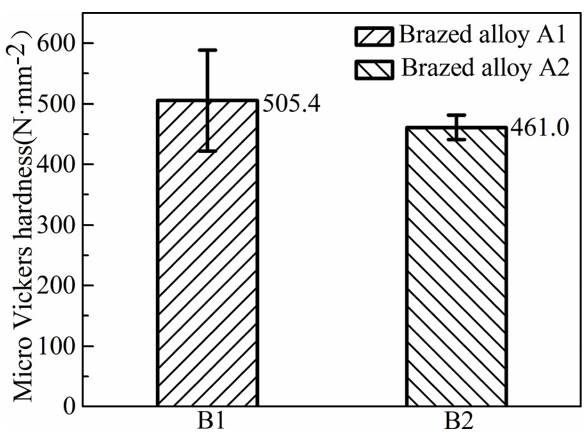

Fig. 6. Micro Vickers hardness of laser brazed layer.

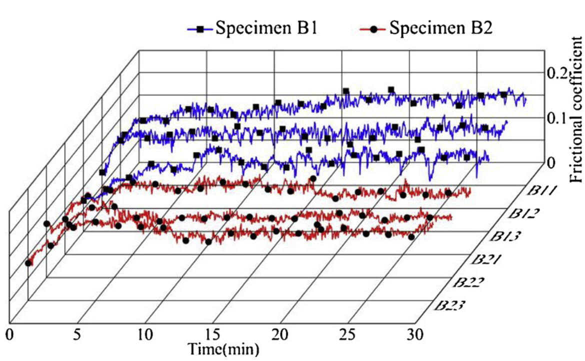

Fig. 7. The friction coefficient curves of specimens B1 and B2.

at the interface, P is the normal load and E′ is the effective elastic modulus of two types of contact materials.

It can be deduced in formula (1) that the smaller the shear stress of τ is, the lesser the friction coefficient will be. Small critical shear stress can reduce the friction coefficient in sliding test. Many types of intermetallic compounds, such as $AgZr_2$, $Cu_{10}Zr_7$, Cu_3Ti and et al., co-existed in the brazed layer can effectively decrease the friction coefficient in the sliding process. The result has good agreements with the published literature [47,48]. Therefore, the integrative friction coefficient between the grinding ball and the brazed layer is decreased with the addition of Zr element. The mean values of the friction coefficients are 0.15 (with Zr element) and 0.18 (without Zr element), respectively.

3.4.2. The wear resistance

Fig. 8 shows the SEM micrographs and three dimensional (3-D) contours of specimens B1 and B2 after sliding tests. The worn track with distinct ridges on both sides can be observed, especially on the specimen B2. It can be explained that the bumped materials at the front beneath the grinding ball had been separated to both sides of the worn groove along the sliding direction to generate the worn track. The accumulation layer of the specimen B1 is discontinuous and with large quantities of small particles, while it is continuous appeared on the specimen B2 and no significant particles close to the worn track, according to the comparison of amplified Fig. 8 (c) and (g). A few obvious grooves at the bottom of the worn tracks can be found in Fig. 8(b) and (f), and the morphology of the grooves shows that the brazed alloys on the specimen B1 has poorer ductility. In addition, pores are observed on the friction and wear surface of the specimen B1. It is indicated that the density of A1 is lower than A2. This is consistent with the section 3. 2. Simultaneously, the compressive ductility of the brazed alloys has been improved with adding the elemental Zr. And the micro-cracks and furrows as well as the particles adhesion have been reduced in sliding test. It can also be seen in Fig. 8(d) and (h) that the worn depth of the specimen B2 is larger than that of the specimen B1 under the same conditions. Mean values of worn volumes are 0.4530 mm^3 and 0.6576 mm^3, respectively. The overall wear resistance of the brazed layers has been slightly decreased with the addition of Zr, and it is still much higher than that of AISI 1045 steel substrate, which is consistent with the above analyzed results for the hardness and compressive ductility of the brazed alloys.

In terms of the friction coefficient and wear volumes of the brazed layers, Zr homogenizes the composition by promoting the formation of more compounds in the brazed alloys. The ductility of the brazed layer has been increased and the friction coefficient has been reduced, which leads to a lower wear resistance occurred on the specimen B2 in sliding test.

By adding active Ti and Zr, AgCu-based alloy, the wettability of $AgCu_{28}$-4.5Ti-4Zr is notably enhanced due to its increment of the ductility. Take the considerations of macroscopic features, intermetallic reaction layers, micro Vickers hardness, as well as tribological performance of the two similar brazed alloys, a prefect compressive performance has been discovered during welding-brazing process and the sliding test. As more intermetallic compounds grow up, the elemental diffusion at the bonding interface is intensified and the chemical metallurgical performance is improved. Additionally, the dominating role of Cu_3Ti in the brazed layer of the specimen B2 is changed due to $AgZr_2$ and $Cu_{10}Zr_7$ been formed. And a smaller friction coefficient is monitored in sliding the brazed layer with the addition of Zr. Though the hardness of the specimen B2 is decreased slightly, a smoother layer with

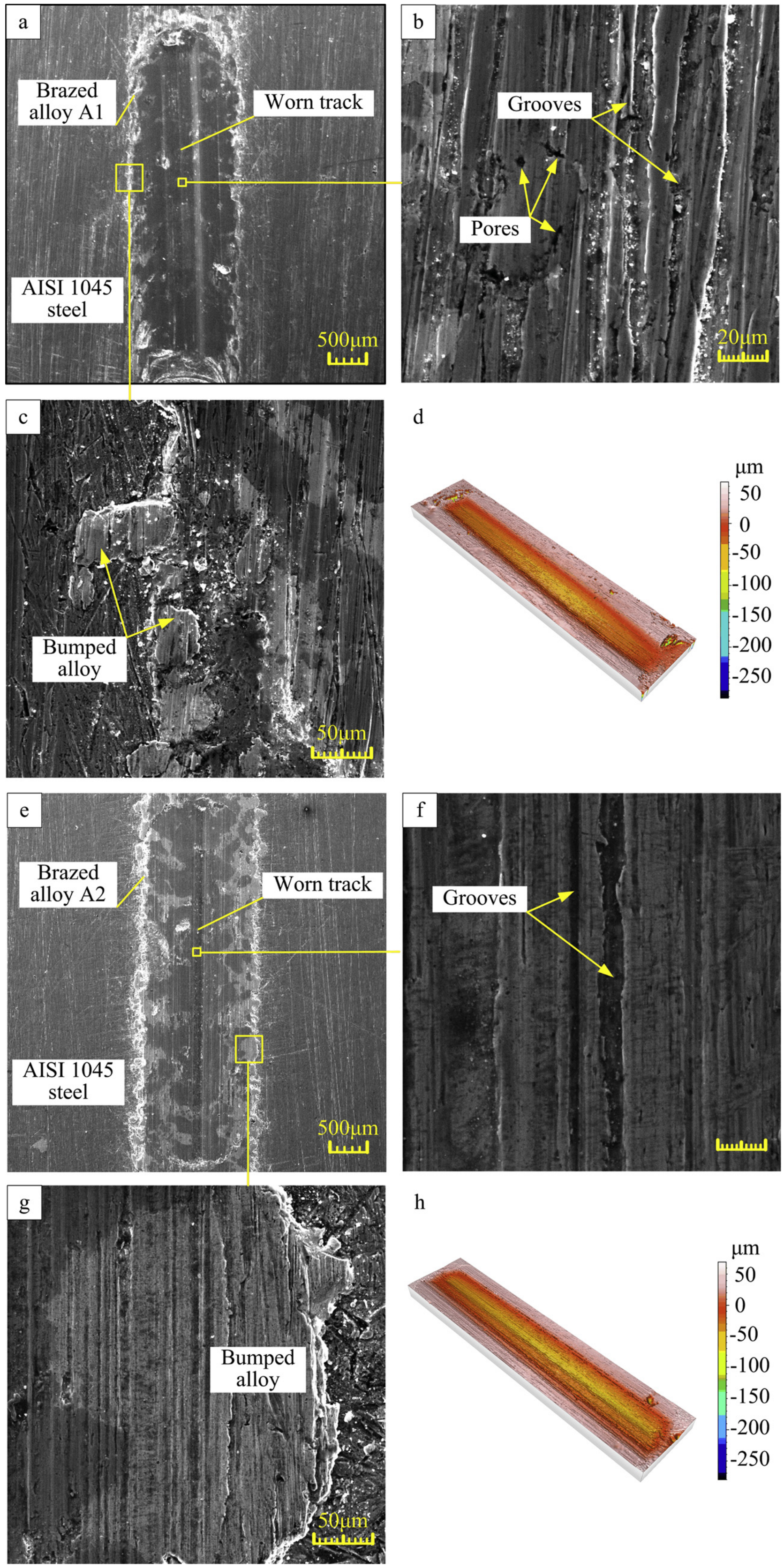

Fig. 8. The SEM micrograph and 3D contours of brazed alloys A1 and A2 after worn: (a) The worn track of specimen B1, (b)The bottom surface of worn track, (c)The accumulation of brazed alloy around the worn track, (d) The 3D contours of worn track; (e) The worn track of specimen B2, (f) The bottom surface of worn track, (g) The accumulation of brazed alloy around the worn track, (h) The 3D contours of worn track.

the enhanced ductility is produced in the welding-brazing process. Wear damage could be weakened in the condition of a smaller friction coefficient between two sliding counterparts.

4. Conclusions

1) Two different plates of AISI 1045 steel and pure Ti have been joined with $AgCu_{28}$-4.5Ti-4Zr active brazing alloys in laser welding-brazing process. The alloys have a good wettability to the matrix, and the brazed layer presents a compact structure and uniform thickness in the connection transition zones.

2) The bidirectional diffusion of main elements occurs when the appropriate amount of Zr has been added in the brazing alloys, and the gradient evolution of elements distribution between brazed layers and matrices has been significantly changed at the transition zones. And the brazed surface tends to be smooth, which improves the metallurgical reaction at the interfaces.

3) Elemental Ti in the Zr-free alloys tends to react with elemental Cu in the transition zones, which can produce the hard-brittle phase Cu_3Ti and result in an uneven brazed layer with characteristics of nonuniform hardness distribution and poor ductility. A few defects, such as micro cracks, furrows and grain adhesion, could be found on the ground surface in sliding tests. The active elemental Zr can inhibit the over-production of hard-brittle phase Cu_3Ti. Fewer phases of Cu_3Ti with new generated phases of $AgZr_2$ and $Cu_{10}Zr_7$ can unify the hardness distribution and improve the tribological performance for the brazed alloy. Furthermore, (Zr, Cu) solid solutions affects the solution strengthening in the brazing process, and it is beneficial to the overall performance.

Author contributions

Yonggui Huang designed the experiment and finished the data analysis by Origin, and completed the paper writing. Professor Guoxing Liang provided the experimental program guidance and revised the first draft of the paper. Professor Ming Lv guided the analysis of experimental data and finalized the draft, and provided good experimental conditions for the research. Al-Nehari Mohammed completed part of the experimental image processing, and also carried on the final revision. Donggang Liu and Guang Li participated in the experiment and obtained the original experimental data. Chun Xiao provided the necessary test conditions for the experiment, and guided some important experiment design simultaneously. All authors contributed have read and approved the final manuscripts.

Funding

This research was funded by National Natural Science Foundation of China (Grant No. 51575375) and Natural Science Foundation of Shanxi Province of China (Grant No. 201801D121174).

Conflicts of interest

The authors declare that we have no financial and personal relationships with other people or organizations that can inappropriately influence the representation or interpretation of reported research results. The funders had no role in the design of the study; in the collection, analyses, or interpretation of data; in the writing of the manuscript, or in the decision to publish the results.

Acknowledgments

The authors thank Mr. Zhang Haiwei and Mr. Lv Zheng for their help in conducting the experiments.

References

[1] Wang Y, Lei K, Ruan Y, Dong W. Microstructure and wear resistance of c-BN/Ni-Cr-Ti composites prepared by spark plasma sintering. Int J Refract Metals Hard Mater 2016;54:98–103. https://doi.org/10.1016/j.ijrmhm.2015.07.010.

[2] Miao Q, Ding WF, Zhu YJ, Chen ZZ, Fu YC. Brazing of CBN grains with Ag-Cu-Ti/TiX composite filler- the effect of TiX particles on microstructure and strength of bonding layer. Mater Design 2016;98:243–53. https://doi.org/10.1016/j.matdes.2016.03.033.

[3] Jackson MJ, Davis CJ, Hitchiner MP, Mills B. High-speed grinding with CBN grinding wheels-applications and future technology. J Mater Process Technol 2001;110(1):78–88. https://doi.org/10.1016/S0924-0136(00)00869-4.

[4] Nicholas MG, Mortimer DA, Jones LM, Crispin RM. Some observations on the wetting and bonding of nitride ceramics. J Mater Sci 1990;25(6):2679–89. https://doi.org/10.1007/BF00584866.

[5] Baghjari SH, Akbarimousavi SAA. Experimental investigation on dissimilar pulsed Nd:YAG laser welding of AISI 420 stainless steel to kovar alloy. Mater Des 2014;57(5):128–34. https://doi.org/10.1016/j.matdes.2013.12.050.

[6] Sepe R, Laiso M, De Luca A, Caputo F. Evaluation of residual stresses in butt welded joint of dissimilar material by FEM. Key Eng Mater 2017;754:268–71. https://doi.org/10.4028/www.scientific.net/KEM.754.268.

[7] Vaidya WV, Horstmann M, Ventzke V, Petrovski B, Koçak M, Kocik R. Structure-property investigations on a laser beam welded dissimilar joint of aluminium AA6056 and titanium Ti6Al4V for aeronautical applications Part I: local gradients in microstructure, hardness and strength. Materwiss Werksttech 2010;40:623–33. https://doi.org/10.1002/mawe.200900366.

[8] Vaidya WV, Horstmann M, Ventzke V, Petrovski B, Koçak M, Kocik R. Structure-property investigations on a laser beam welded dissimilar joint of aluminium AA6056 and titanium Ti6Al4V for aeronautical applications. Part II: resistance to fatigue crack propagation and fracture. Materwiss Werksttech 2010;40:769–79. https://doi.org/10.1002/mawe.200900367.

[9] Meco S, Pardal G, Ganguly S, Williams S, McPherson N. Application of laser in seam welding of dissimilar steel to aluminium joints for thick structural components. Opt Lasers Eng 2015;67:22–30. https://doi.org/10.1016/j.optlaseng.2014.10.006.

[10] Elrefaey A, Tillmann W. Solid state diffusion bonding of titanium to steel using a copper base alloy as interlayer. J Mater Process Technol 2009;209(5):2746–52. https://doi.org/10.1016/j.jmatprotec.2008.06.014.

[11] Lee MK, Lee JG, Choi YH, Kim DW, Rhee CK, Lee YB, et al. Interlayer engineering for dissimilar bonding of titanium to stainless steel. Mater Lett 2010;64(9):1105–8. https://doi.org/10.1016/j.matlet.2010.02.024.

[12] Atasoy E, Kahraman N. Diffusion bonding of commercially pure titanium to low carbon steel using a silver interlayer. Mater Charact 2008;59(10):1481–90. https://doi.org/10.1016/j.matchar.2008.01.015.

[13] Shen Q, Xiang HY, Luo GQ, Wang CB, Li MJ, Zhang LM. Microstructure and mechanical properties of TC4/oxygen-free copper joint with silver interlayer prepared by diffusion bonding. Mater Sci Eng A 2014;596:45–51. https://doi.org/10.1016/j.msea.2013.12.017.

[14] Zhang Y, Sun DQ, Gu XY, Li HM. Nd:YAG pulsed laser welding of dissimilar metals of titanium alloy to stainless steel. Int J Adv Manuf Technol 2018;94(1-4):1073–85. https://doi.org/10.1007/s00170-017-0997-3.

[15] Ding WF, Xu JH, Shen M, Su HH, Fu YC, Xiao B. Joining of CBN abrasive grains to medium carbon steel with Ag–Cu/Ti powder mixture as active brazing alloy. Mater Sci Eng A 2006;430(1-2):301–6. https://doi.org/10.1016/j.msea.2006.05.057.

[16] Xiao DH, Li XX, Zhang FQ, Zhang YS. Effect of Zr addition on microstructure and properties of Cu–Ag–Ti alloys. J Mater Eng Perform 2014;23(5):1854–60. https://doi.org/10.1007/s11665-014-0926-7.

[17] Luo JG, Acoff VL. Interfacial reactions of titanium and aluminum during diffusion welding. Weld J 2000;79. 239-s-43-s.

[18] Kim YC, Fuji A. Factors dominating joint characteristics in Ti-Al friction welds. Sci Technol Weld Join 2002;7(3):149–54. https://doi.org/10.1179/136217102225004185.

[19] Borrisutthekul R, Yachi T, Miyashita Y, Mutohc Y. Suppression of intermetallic reaction layer formation by controlling heat flow in dissimilar joining of steel and aluminum alloy. Mater Sci Eng A 2007;467:108–13. https://doi.org/10.1016/j.msea.2007.03.049.

[20] Peyre P, Sierra G, Deschaux-Beaume F, Stuart D, Fras G. Generation of aluminium–steel joints with laser-induced reactive wetting. Mater Sci Eng A. 2007;444:327–38. https://doi.org/10.1016/j.msea.2006.09.111.

[21] Chen YC, Nakata K. Microstructural characterization and mechanical properties in friction stir welding of aluminum and titanium dissimilar alloys. Mater Des 2009;30(3):469–74. https://doi.org/10.1016/j.matdes.2008.06.008.

[22] Dezellus O, Andrieux J, Bosselet F, Sacerdote-Peronnet M, Baffie T, Hodaj F, et al. Transient liquid phase bonding of titanium to aluminum nitride. Mater Sci Eng A 2008;495:254–8. https://doi.org/10.1016/j.msea.2007.10.104.

[23] Liu XB, Pang M, Guo J, Yu G. Transmission electron microscopy characterization of laser welding cast Ni-based superalloy K418 turbo disk and alloy steel 42CrMo shaft. J Alloys Compd 2008;461(1-2):648–53. https://doi.org/10.1016/j.jallcom.2007.07.079.

[24] Chen HC, Bi G, Bing YL, Cheng CK. Laser welding of CP Ti to stainless steel with different temporal pulse shapes. J Mater Process Technol 2016;231:58–65. https://doi.org/10.1016/j.jmatprotec.2015.12.016.

[25] Sechi Yoshihisa, Tsumura T, Nakata K. Dissimilar laser brazing of boron nitride and tungsten carbide. Mater Des 2010;31(4):2071–7. https://doi.org/10.1016/j.matdes.2009.10.009.

[26] Borrsutthekul R, Yachi T, Miyashita Y, Mutoh Y. Suppression of intermetallic

reaction layer formation by controlling heat flow in dissimilar joining of steel and aluminum alloy. Mater Sci Eng A 2007;467:108–13. https://doi.org/10.1016/j.msea.2007.03.049.
[27] Sierra G, Peyre P, Deschaux Beaume F, Stuart D, Fras G. Steel to aluminium braze welding by laser process with Al-12Si filler wire. Sci Technol Weld Join 2008;13:430–7. https://doi.org/10.1179/174329308X341852.
[28] Kreimeyer M, Wagner F, Vollertsen F. Laser processing of aluminum-titanium-tailored blanks. Opt Lasers Eng 2005;43(9):1021–35. https://doi.org/10.1016/j.optlaseng.2004.07.005.
[29] Qixun PAN. Some problems should be paid attention to in the manufacture and use of diamond abrasive tools. Construction Mechanization 1992;5:20–3. https://doi.org/10.13311/j.cnki.conmec.1992.05.007. (In Chinese).
[30] Qian N, Ding WF, Zhu YJ. Comparative investigation on grindability of K4125 and Inconel718 nickel-based superalloys. Int J Adv Manuf Technol 2018;97:1649–61. https://doi.org/10.1007/s00170-018-1993-y.
[31] Ding WF, Xu JH, Chen ZZ, Su HH, Fu YC. Wear behavior and mechanism of single-layer brazed CBN abrasive wheels during creep-feed grinding cast nickel-based superalloy. Int J Adv Manuf Technol 2010;51:541–50. https://doi.org/10.1007/s00170-010-2643-1.
[32] Ghosh A, Chattopadhyay AK. Performance enhancement of single-layer miniature cBN wheels using CFUBMS-deposited TiN coating. Int J Mach Tools Manuf 2007;47(12-13):1799–806. https://doi.org/10.1016/j.ijmachtools.2007.04.008.
[33] Paul S, Chattopadhyay AB. Effects of cryogenic cooling by liquid nitrogen jet on forces, temperature and surface residual stresses in grinding steels. Cryogenics 1995;35(8):515–23. https://doi.org/10.1016/0011-2275(95)98219-Q.
[34] Bhaduri D, Kumar R, Jain AK, Chattopadhyay AK. On tribological behaviour and application of TiN and MoS2-Ti composite coating for enhancing performance of monolayer cBN grinding wheel. Wear 2010;268:1053–65. https://doi.org/10.1016/j.wear.2010.01.013.
[35] Xu W, Zhu YJ, Du BC Ding WF. Residual stresses of polycrystalline CBN abrasive grits brazed with a high-frequency induction heating technique. Chin J Aeronaut 2018. https://doi.org/10.1016/j.cja.2018.07.008.
[36] Wang JW, Yu TY, Ding WF, Fu YC, Ashraf F, Bastawros. Wear evolution and stress distribution of single CBN superabrasive grain in high-speed grinding. Precis Eng 2018;54:70–80. https://doi.org/10.1016/j.precisioneng.2018.05.003.
[37] Zhou H, Ding WF, Liu CJ. Material removal mechanism of PTMCs in high-speed grinding when considering consecutive action of two abrasive grains. Int J Adv Manuf Technol 2018;07:1–13. https://doi.org/10.1007/s00170-018-2685-3.
[38] Ghosh A, Chattopadhyay AK. Interfacial reaction and wetting behavior of active Ag-Cu filler alloys on surface of cBN grits and its influence on failure patterns of brazed joint. Int J Refract Met Hard Mater 2017;68:96–103. https://doi.org/10.1016/j.ijrmhm.2017.07.002.
[39] Liang GX, Schmauder S, Lv M, Schneider YL, Zhang C, Han Y. An investigation of the influence of initial roughness on the friction and wear behavior of ground surfaces. Materials 2018;11(2):237–58. https://doi.org/10.3390/ma11020237.
[40] Louzguine DV, Kato H, Inoue A. High-strength Cu-based crystal-glassy composite with enhanced ductility. Appl Phys Lett 2004;84(7):1088–9. https://doi.org/10.1063/1.1647278.
[41] Ollivier M, Harker RM, Gourlay CM. Reaction-induced surface reconstruction of silver in contact with zirconium. J Alloys Compd 2017;691:624–33. https://doi.org/10.1016/j.jallcom.2016.08.282.
[42] Chu QL, Zhang M, Li JH, Fan QY, Xie WW, Bi ZY. Joining of CP-Ti/Q345 sheets by Cu-based filler metal and effect on interface. J Mater Process Technol 2015;225:67–76. https://doi.org/10.1016/j.jmatprotec.2015.05.017Get. rights and content.
[43] Simhan DR, Ghosh A. Vacuum brazing of cubic boron nitride to medium carbon steel with Zr added passive and Ti activated eutectic Ag-Cu alloys. Ceram Int 2018;44:4891–9. https://doi.org/10.1016/j.ceramint.2017.12.079.
[44] Wang YR, Wang YQ, Hui ZP, Song J. Mechanical properties of AISI 1045 ceramic coated materials by nano indentation and crack opening displacement method. J Cent South Univ 2012;19:3023–7. https://doi.org/10.1007/s11771-012-1373-y.
[45] Liu HY, Fine M. Tribological behavior of SiC whisker/Al2O3 composites against carburized 8620 steel in lubrication sliding. J Am Ceram Soc 1991;74(9):2224–33. https://doi.org/10.1111/j.1151-2916.1991.tb08289.x.
[46] Yin ZB, Yuan JT, Huang CZ, Wang ZH, Huang L, Cheng Y. Friction and wear behaviors of Al2O3/TiC micro-nano-composite ceramic sliding against metals and hard materials. Ceram Int 2016;42(1):1982–9. https://doi.org/10.1016/j.ceramint.2015.10.001.
[47] Wesmann JAR, Espallargas N. Effect of atmosphere, temperature and carbide size on the sliding friction of self-mated HVOF WC-CoCr contacts. Tribol Int 2016;101:301–13. https://doi.org/10.1016/j.triboint.2016.04.032.
[48] Deng JX, Zhang H, Wu Z, Lian YS, Zhao J. Friction and wear behaviors of WC/Co cemented carbide tool materials with different WC grain sizes at temperatures up to 600 °C. Int J Refract Met Hard Mater 2012;31:196–204. https://doi.org/10.1016/j.ijrmhm.2011.11.003.